

Bayesian State Space Modeling of Physical Processes in Industrial Hygiene

Nada Abdalla

Department of Biostatistics, University of California-Los Angeles.

Sudipto Banerjee

Department of Biostatistics, University of California-Los Angeles.

Gurumurthy Ramachandran

Department of Environmental Health and Engineering,
Bloomberg School of Public Health, Johns Hopkins University.

Susan Arnold

Division of Environmental Health Sciences, School of Public Health,
University of Minnesota.

July 9, 2018

Abstract

Exposure assessment models are deterministic models derived from physical-chemical laws. In real workplace settings, chemical concentration measurements can be noisy and indirectly measured. In addition, inference on important parameters such as generation and ventilation rates are usually of interest since they are difficult to obtain. In this paper we outline a flexible Bayesian framework for parameter inference and exposure prediction. In particular, we devise Bayesian state space models by discretizing the differential equation models and incorporating information from observed measurements and expert prior knowledge. At each time point, a new measurement is available that contains some noise, so using the physical model and the available measurements, we try to obtain a more accurate state estimate, which can be called filtering. We consider Monte Carlo sampling methods for parameter estimation and inference under nonlinear and non-Gaussian assumptions. The performance of the different methods is studied on computer-simulated and controlled laboratory-generated data. We consider some commonly used exposure models representing different physical hypotheses.

Keywords: Bayesian modeling; Eddy-diffusion; Exposure assessment; Industrial hygiene; Kalman filters; Physical Models; State-Space Modeling; Two-zone model; Well-mixed model.

technometrics tex template (do not remove)

1 Introduction

In industrial hygiene, estimation of a worker’s exposure to chemical concentrations in the workplace is an important concern. In many situations, chemical concentrations are unobserved directly and partial noisy measurements are available. Exposure models aim at capturing the underlying physical processes generating chemical concentrations in the workplace. Exposure modeling through statistical and mathematical models may provide more accurate exposure estimates than monitoring (Nicas and Jayjock, 2002). Industrial hygienists seek to infer these latent processes from the available measurements as well as quantification of uncertainty in parameter estimation. For example, generation and ventilation rates are crucial parameters that are difficult to obtain since most workplaces do not collect information routinely. Traditional approaches involve using deterministic physical models that ignore the existence of uncertainty by assigning values to those parameters (Keil et al., 2009). These approaches however don’t provide accurate representation in a real workplace environment. Bayesian methods combining professional judgment from experts and direct measurements (Gelman et al., 2013) were successful in different settings (Banerjee et al., 2014). For example, Zhang et al. (2009) introduced a nonlinear regression on the solution of the differential equations representing the underlying physical model within a Bayesian setting for the two-zone model using Gaussian errors. The model has some limitations since it ignores extraneous factors and variations and requires a closed-form solution of the differential equations. This severely limits the number of applicable physical models. Monteiro et al. (2011) introduced an R package (B2Z), which implements the Bayesian two-zone model proposed by Zhang et al. (2009). Monteiro et al. (2014) demonstrated that straightforward Bayesian regression can be ineffective in predicting exposure concentrations in industrial workplaces since the information is limited to partial measurements. They introduced a process-based Bayesian melding approach where measurements are related to the physical model through a stochastic process that captures the bias in the physical model and a measurement error. The resulting inference suffers from inflated variability because of the additional complexities in the model, cumbersome computations and opaque interpretation.

Physical models for industrial hygiene are represented by differential equations that

model the rate of change in concentrations. We propose using Bayesian state space models by discretizing the physical model differential equations and incorporating information from observed measurements and experts prior knowledge. This approach will enrich the existing methods, as industrial hygienists will no longer be restricted to fitting a confined selection of physical models amenable to analytic solutions. Any conceivable physical model, in theory, can be accommodated. Neither will they be restricted to Gaussian data, an assumption that most industrial hygiene practitioners will agree is rarely tenable, especially given the small to moderate number of measurements they have to deal with.

At each time point, a new measurement is available that contains some noise, so using the physical model and the available measurements, we try to obtain a more accurate state estimate, which can be called filtering. The importance of filters lies in their ability to produce estimates of the latent process using information generated by the observations which may provide a poor representation of the latent process if used alone. The aim is to infer the latent process using those observations, along with the physical model that theoretically describes it, as well as incorporating professional knowledge. We consider Monte Carlo based filtering methods for parameter estimation and inference in state space models. We also relax the assumption of Gaussian error terms and consider other alternatives.

In particular, we consider different filtering methods under different assumptions. The widely deployed Kalman filter (KF) (Eubank, 2005) offers an optimal solution under linearity and normality assumptions. State-by-state update sampler (Fearnhead, 2011) can provide state estimates under nonlinear and/or non-Gaussian models. The different models are compared and assessed using computer-simulated data and lab-generated data. In the lab-generated data, most of the model parameters are known up to a considerable level of accuracy. Experiments were conducted in a controlled chamber that mimics real workplace settings where concentrations were generated at different ventilation and generation rates and under different exposure physical models.

Our contribution in this article expands upon the existing exposure models to allow for better prediction of the quantities of interest. The article is organized as follows. Section 2 provides a brief review of three families of commonly referenced exposure physical models. Section 3 describes the Bayesian approaches used. Section 4 illustrates our model through

applying it to the simulated data and lab-generated data. Section 5 concludes the article suggesting some future work.

2 Physical models and their statistical counterparts

Bayesian state space representations for exposure assessment models combine direct measurements of the environmental exposure, physical models and prior information. There are several physical models varying in their level of complexity (Ramachandran, 2005). Three commonly used families of physical models are the well-mixed compartment (one-zone) model, the two-zone model and the turbulent eddy diffusion model. We use discrete approximations to the deterministic physical models and introduce stochastic error terms to derive corresponding dynamic statistical models. This obviates the need for exact analytic solutions to the differential equations, which can be sensitive to the choice of initial conditions. Prior specifications for the model parameters produce Bayesian state space models (SSMs).

Dynamic steady-state models combine measurements with the true underlying state. They are composed of (i) a measurement equation that relates the observations (or some function thereof) to the true concentrations; and (ii) a transition equation describing the concentration change from time t to time $t + \delta_t$. We will derive the dynamic models from the respective differential equations for three popular physical models in industrial hygiene.

2.1 Well-mixed compartment (one-zone) model

The well-mixed compartment model assumes that a source is generating a pollutant at a rate G (mg/min) in a room of volume V (m³) with ventilation rate Q (m³/min). The room is assumed to be perfectly mixed, which means that there is a uniform concentration of the contaminant throughout the room (Figure 1). The loss term K_L (mg/min) measures the loss rate of the contaminant due to other factors such as chemical reactions or the contaminant being absorbed by the room surfaces.

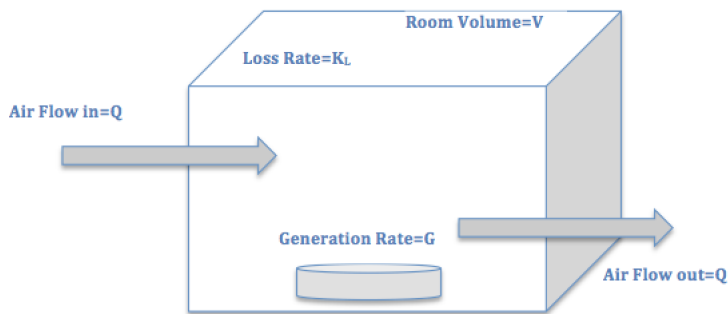


Figure 1: One-zone model schematic showing key model parameters; generation rate G , ventilation rate Q and loss rate K_L

The differential equation describing this model is

$$V \frac{d}{dt} C(t) + (Q + K_L V) C(t) = G . \quad (1)$$

The solution to the differential equation is

$$C(t) = \exp\{-t(Q+K_L V)/V\} C(t_0) + ((Q + K_L V)/V)^{-1} [1 - \exp\{-t(Q + K_L V)/V\}] G/V . \quad (2)$$

Theoretically, the steady state concentration is the limit of $C(t)$ as $t \rightarrow \infty$ which is G/Q (mg/m^3). Details of the steady state solution are provided in the supplementary material. Further specifications yield the Bayesian SSM corresponding to (1). For example,

$$\begin{aligned} \text{Measurement: } Z_t &= f(C_t) + \nu_t , \quad \nu_t \stackrel{iid}{\sim} P_{\nu, \theta_\nu} ; \\ \text{Transition: } C_{t+\delta t} &= \left(1 - \delta t \frac{Q + K_L V}{V}\right) C_t + \delta t \frac{G}{V} + \omega_t , \quad \omega_t \stackrel{iid}{\sim} P_{\omega, \theta_\omega} . \\ Q &\sim \text{Unif}(a_Q, b_Q) ; \quad G \sim \text{Unif}(a_G, b_G) ; \quad K_L \sim \text{Unif}(a_{K_L}, b_{K_L}) ; \quad \sigma^2 \sim \text{IG}(a_\sigma, b_\sigma) ; \end{aligned} \quad (3)$$

where Z_t represents measurements (perhaps transformed), $f(\cdot)$ is a function that maps C_t to the scale of Z_t , P_{ν, θ_ν} and $P_{\omega, \theta_\omega}$ are probability distributions to be specified, while the prior distributions for the physical parameters are customarily specified as uniform within certain fixed physical bounds.

2.2 Two-zone model

The two zone model assumes the presence of a source for the contaminant in the workplace. Two zones or regions are defined: (i) the region closer to the source is called the “*near field*”, while the rest of the room is called the far “*far field*”, which completely encloses the near field. Both fields are assumed to be a well-mixed box, i.e., two distinct places that are in the same field have equal levels of concentration of the contaminant. Similar to the one-zone model, this model assumes that a contaminant is generated at a rate $G(\text{mg}/\text{min})$, in a room with supply and exhaust flow rates (ventilation rate) $Q(\text{m}^3/\text{min})$ and loss rate by other mechanisms $K_L(\text{mg}/\text{m}^3)$. This model includes one more parameter that indicates the airflow between the near and the far field $\beta(\text{m}^3/\text{min})$. The volume in the near field is denoted by $V_N(\text{m}^3)$ and the volume in the far field is denoted by $V_F(\text{m}^3)$. Figure 2 illustrates the dynamics of the system.

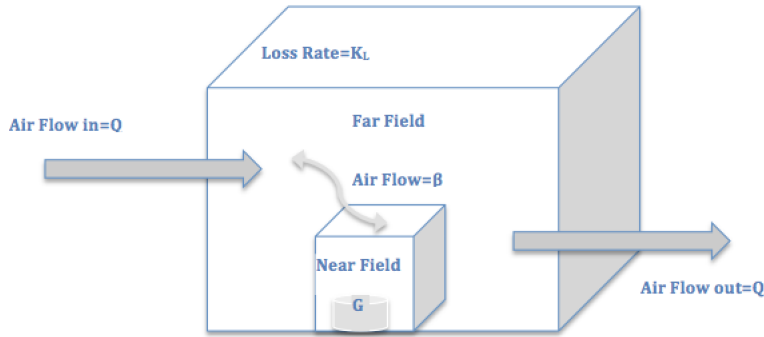


Figure 2: Two-zone model schematic showing key model parameters; generation rate G , ventilation rate Q , airflow β and loss rate K_L

The following system of differential equations represents the two-zone model

$$\overbrace{\frac{d}{dt} \begin{bmatrix} C_N(t) \\ C_F(t) \end{bmatrix}}^{\frac{d}{dt} C(t)} = \overbrace{\begin{bmatrix} -\beta/V_N & \beta/V_N \\ \beta/V_F & -(\beta + Q)/V_F + K_L \end{bmatrix}}^A \overbrace{\begin{bmatrix} C_N(t) \\ C_F(t) \end{bmatrix}}^{C(t)} + \overbrace{\begin{bmatrix} G/V_N \\ 0 \end{bmatrix}}^g. \quad (4)$$

The solution to the differential equations is

$$C(t) = \exp(tA)C(t_0) + A^{-1} [\exp(tA) - I] g , \quad (5)$$

where $\exp(tA)$ is the matrix exponential. Theoretically, for large values of t , the steady state concentration in the near field is $G/Q + G/\beta$ (mg/m³), and G/Q (mg/m³) in the far field. We note that the matrix exponential may be numerically unstable to compute in general. For example, for non-diagonalizable matrices a Jordan decomposition (see, e.g., Banerjee and Roy, 2014) may be required, which is very sensitive to small perturbations in the elements of A . Hence, we will avoid this approach.

Analogous to (3), the discrete counterpart of (4) can be

$$\text{Measurement: } Z_t = f(C_t) + \nu_t, \quad \nu_t \stackrel{iid}{\sim} P_{\nu_t, \theta_\nu} ;$$

$$\text{Transition: } C_{t+\delta t} = (\delta_t A(\theta_c; x) + I) C_t + \delta_t g(\theta_c; x) + \omega_t ; \quad \omega_t \stackrel{iid}{\sim} P_{\omega_t, \theta_\omega} ;$$

$$Q \sim Unif(a_Q, b_Q) ; \quad G \sim Unif(a_G, b_G) ; \quad K_L \sim Unif(a_{K_L}, b_{K_L}) ; \quad \beta \sim Unif(a_\beta, b_\beta) ,$$

where Z_t is the 2×1 vector with near-field and far-field measurements (or some function thereof) at time t , C_t is the unobserved concentration state at time t , $A(\theta_c; x) = \begin{bmatrix} -\beta/V_N & \beta/V_N \\ \beta/V_F & -(\beta + Q)/V_F + K_L \end{bmatrix}$ and $g(\theta_c; x) = \begin{bmatrix} G/V_N \\ 0 \end{bmatrix}$. Similar to the one-zone model, we will specify distributions for ν_t and for ω_t , where θ_ν and θ_ω are parameters in P_{ν, θ_ν} and $P_{\omega, \theta_\omega}$, respectively.

2.3 Turbulent eddy diffusion model

In real workplace settings, the rooms may neither be perfectly mixed nor consist of well-mixed zones. Furthermore, the concentration state could depend upon space and time. A popular model for such settings is the turbulent eddy diffusion model. This model accounts for a continuous concentration gradient from the source outward. It takes into account the worker's location relative to the source. The concentration $C(s, t)$ is a function of the location $s = (x, y)$ in a two-dimensional Euclidean coordinate frame and time t . Without loss of generality, the source of the contaminant is assumed to be at coordinate

(0, 0). The parameter that is unique to this model is the turbulent eddy diffusion coefficient $D_T(\text{m}^2/\text{min})$. It describes how quickly the emission spreads with time (Figure 3) and is assumed to be constant over space and time. There has been very little research on the

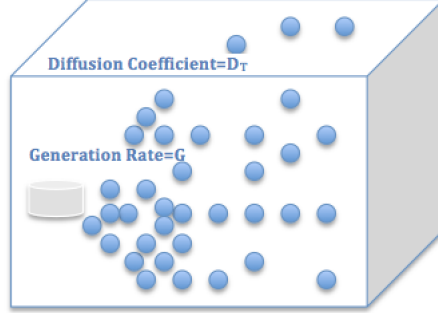


Figure 3: Eddy diffusion model schematic showing key model parameter; diffusion coefficient D_T

values of D_T due to the difficulty of measuring it. Some studies suggest a relationship between D_T and air change per hour (ACH) (Shao et al., 2017). We will provide inference for this parameter.

The exact contaminant concentration at location s relative to the source of emission is

$$C(s, t) = \frac{G}{2\pi D_T \|s\|} \left\{ 1 - \text{erf} \left(\frac{\|s\|}{\sqrt{4D_T t}} \right) \right\}, \quad (6)$$

where $\text{erf}(z) = \frac{2}{\pi} \int_0^z \exp(-u^2) du$. The steady state concentration at location s is theoretically the limit of the concentration as $t \rightarrow \infty$, which is $G/(2\pi D_T(s))$ (mg/m^3).

The following differential equation represents the change in concentration over time

$$\frac{d}{dt} C(s, t) = \frac{G}{4(D_T \pi t)^{3/2}} \exp(-\|s\|^2/4D_T t).$$

A general dynamic modeling framework accounting for space and time is as follows:

Measurement: $Z(t, s) = f(C(t, s)) + \nu_t(s) + \eta_t$, $\nu_t(s) \sim P_{\nu_t(s), \theta_\nu}$, $\eta_t \sim P_{\eta_t, \theta_\eta}$;

Transition: $C(s, t + \delta_t) = C(s, t) + \delta_t \frac{G}{4(D_T \pi t)^{3/2}} \exp(-\|s\|^2/4D_T t) + \omega(s, t + \delta_t)$, $\omega(s, t) \sim P_{\omega_t, s, \theta_\omega}$;

$D_T \sim \text{Unif}(a_{D_T}, b_{D_T})$; $G \sim \text{Unif}(a_G, b_G)$, (7)

where $P_{\nu_t(s),\theta_\nu}$ and $P_{\omega_t,s,\theta_\omega}$ are spatial-temporal stochastic processes. Note that $\nu_t(s)$ is a spatial-temporal process discrete in time and continuous in space. This is reasonable because the measurements are taken over discrete time intervals and the estimation for the latent concentration states are required at those intervals. On the other hand, $\omega(s,t)$ would ideally be a process continuous in both space and time because it models spatial-temporal associations between concentration states at arbitrary space-time coordinates.

3 Model Implementation and Assessment

For each physical model in Section 2 we will consider two different Bayesian SSMs. We will refer to the first as a Gaussian SSM. Gaussian (linear) SSMs result from specifying $f(C_t) = B_t C_t$, where B_t is a known $p \times p$ design matrix (usually the identity matrix), $P_{\nu,\theta_\nu} \equiv N(0, \Sigma_\nu)$ and $P_{\omega,\theta_\omega} \equiv N(0, \Sigma_\omega)$ are p -variate Gaussian densities. These deliver accessible distribution theory for updating parameters using Kalman-filters or Gibbs samplers. Let $\mathcal{T} = \{t_1, \dots, t_n\}$ be timepoints where concentration measurements Z_t have been measured. A Bayesian hierarchical SSM is

$$p(\theta_c) \times IW(\Sigma_\omega | r_\omega, S_\omega) \times IW(\Sigma_\nu | r_\nu, S_\nu) \times N(C_{t_0} | m_0, \Sigma_0) \\ \times \prod_{i=1}^n N(C_{t_i} | A_{t_i}(\theta_c)C_{t_{i-1}} + \delta_i g_{t_i}, \Sigma_\omega) \times \prod_{i=1}^n N(Z_{t_i} | B_{t_i}C_{t_i}, \Sigma_\nu), \quad (8)$$

where $p(\theta_c)$ is the prior distribution on θ_c , $\delta_i = t_i - t_{i-1}$, and the other distributions follow definitions as in Gelman et al. (2013). Gibbs updates are implemented using $p(C_{t_i} | \cdot) = N(C_{t_i} | M_{t_i} m_{t_i}, M_{t_i})$, where $m_{t_i} = \Sigma_\nu^{-1} Z_{t_i} + \Sigma_{t_i|t_{i-1}}^{-1} A_{t_i}(\theta_c) C_{t_{i-1}}$ and $M_{t_i} = (\Sigma_\nu^{-1} + \Sigma_{t_i|t_{i-1}}^{-1})^{-1}$, where $\Sigma_{t_i|t_{i-1}} = A_{t_i}(\theta_c) M_{t_{i-1}} A_{t_i}(\theta_c)^T + \Sigma_\omega$ and $M_{t_0} = \Sigma_0$, $p(\Sigma_\nu | \cdot) = IW(\Sigma_\nu | r_{\nu|\cdot}, S_{\nu|\cdot})$ and $p(\Sigma_\omega | \cdot) = IW(\Sigma_\omega | r_{\omega|\cdot}, S_{\omega|\cdot})$, where $r_{\nu|\cdot} = r_\nu + n$, $S_{\nu|\cdot} = S_\nu + \sum_{i=1}^n (Z_{t_i} - B_{t_i} C_{t_i})(Z_{t_i} - B_{t_i} C_{t_i})^T$, $r_{\omega|\cdot} = r_\omega + n$ and $S_{\omega|\cdot} = S_\omega + \sum_{i=1}^n (C_{t_i} - A_{t_i}(\theta_c) C_{t_{i-1}})(C_{t_i} - A_{t_i}(\theta_c) C_{t_{i-1}})^T$.

Note that the two-zone model has $p = 2$, while the one-compartment and eddy-diffusion models have $p = 1$. Gaussian Bayesian SSMs for $p = 1$ specify $P_{\nu,\theta_\nu} \equiv N(0, \sigma^2)$ and $P_{\omega,\theta_\omega} \equiv N(0, \tau^2)$. The measurement equation is linear in the state C_t . The $IW(\cdot, \cdot)$ priors in (8) are replaced by $IG(\sigma^2 | a_\sigma, b_\sigma)$ and $IG(\tau^2 | a_\tau, b_\tau)$. The full conditionals now assume

the form $p(C_{t_i} | \cdot) = N(C_{t_i} | M_{t_i} m_{t_i}, M_{t_i})$, where $m_{t_i} = \sigma^{-2} Z_{t_i} + \sigma_{t_i|t_{i-1}}^{-2} A_{t_i}(\theta_c) C_{t_{i-1}}$ and $M_{t_i} = 1/(\sigma^{-2} + \sigma_{t_i|t_{i-1}}^{-2})$, where $\sigma_{t_i|t_{i-1}}^2 = A_{t_i}(\theta_c)^2 M_{t_{i-1}} + \tau^2$, $p(\sigma^2 | \cdot) = IG(\sigma^2 | a_{\sigma|\cdot}, b_{\sigma|\cdot})$ and $p(\tau^2 | \cdot) = IG(\tau^2 | a_{\tau|\cdot}, b_{\tau|\cdot})$, where $a_{\sigma|\cdot} = a_\sigma + n/2$, $b_{\sigma|\cdot} = b_\sigma + \sum_{i=1}^n (Z_{t_i} - B_{t_i} C_{t_i})^2/2$, $a_{\tau|\cdot} = a_\tau + n/2$ and $b_{\tau|\cdot} = b_\tau + \sum_{i=1}^n (C_{t_i} - A_{t_i}(\theta_c) C_{t_{i-1}})^2/2$.

Although Gaussian SSMs are very popular in dynamic modeling of physical systems, especially due to convenient updating schemes, the Gaussian assumption for the concentration measurements may be untenable. Our second Bayesian SSM assumes that $Z_t = \log Y_t$ are log-concentration measurements and $f(C_t) = \log C_t$ in the measurement equation. We still specify P_{ν, θ_ν} as Gaussian, which means that Z_t 's are log-normal and is probably a more plausible assumption than in Gaussian SSMs. In the transition equation, again the Gaussian assumption on ω_t seems implausible: if the measurements of the state are log-normal, then why should C_t be Gaussian? Since C_t is positive, a Gamma or log-normal specification for $P_{\omega, \theta_\omega}$ seems much more plausible. For $p = 2$, we will specify logarithmic bivariate normal distributions, while for $p = 1$ we will explore with both Gamma and log-normal densities. We will refer to all of these models as non-Gaussian Bayesian SSMs.

The turbulent eddy-diffusion model requires some further specifications. While the framework in (7) is rich, unfortunately it will not usually be applicable to practical industrial hygiene settings because typically very few measurements are available over distinct locations in a workplace chamber and estimating the processes will be unfeasible. Hence, we will need simpler specifications. For example, we can consider a setting with locations $\{s_1, s_2, \dots, s_m\}$ and n time-points. We fit the model in (7) with $Z_t(s_i) = \log Y_t(s_i)$ are log-concentration measurements and $f(C_t(s_i)) = \log C_t(s_i)$. We further specify P_{η_t, θ_η} as a white-noise process, i.e., $\eta_t \stackrel{iid}{\sim} N(0, \tau^2)$ for every t and s , and $P_{\nu_t(s), \theta_\nu}$ is a temporally indexed spatial Gaussian process with an exponential covariance function, independent across time. This means that the $m \times 1$ vector $\nu_t \stackrel{ind}{\sim} N(0, \sigma_t^2 R_t(\phi_t))$, where $R_t(\phi_t)$ is an $m \times m$ matrix with (i, j) -th element $\exp(-\phi_t d_{ij})$ and $d_{ij} = \|s_i - s_j\|$.

Note that $P_{\nu_t(s), \theta_\nu}$ can, in theory, be a continuous-time spatial-temporal process specified through a space-time covariance function (see, e.g., Banerjee et al., 2014). Alternatively, one could treat time as discrete and evolving, for each location s , as an autoregressive process so that $\nu_t(s) = \gamma \nu_{t-1}(s) + \eta_t(s)$ with $\eta_t(s)$ being spatial processes independent across time (see,

e.g., Wikle and Cressie, 1999; Gelfand et al., 2005). One could continue to embellish the model in (7) using spatial-temporal structures that represent richer hypotheses and more flexible modeling. However, in realistic industrial hygiene applications such specifications will rarely lead to estimable models given the scarcity of data points. For example, most settings will provide measurements from only a handful of locations (e.g., $m \sim 5$) and some moderate numbers of time points (e.g., $n \sim 100$). Therefore, we will not explore these specifications any further. Moreover, even when we assume independence across time it will be difficult to estimate models with time-varying spatial process parameters. Hence, we let $\nu_t \stackrel{iid}{\sim} N(0, \sigma^2 R(\phi))$ so that each $m \times 1$ vector ν_t has the same m -variate Gaussian distribution.

Finally, we turn to smoothing and filtering. Smoothing is achieved by evaluating at each time point t_i the posterior expectation of the concentration value given the entire observed data $y = \{y_{t_i} : i = 1, 2, \dots, n\}$, including observations before and after t_i . Thus, we sample from the posterior density $p(C_{t_i} | y)$ in posterior predictive fashion by sampling a C_{t_i} from its full conditional, $p(C_{t_i} | \cdot)$, for each sampled value of the parameters. For linear Gaussian SSM, Kalman smoother can be used where the smoothed distribution at time t also follows a Gaussian distribution. For the nonlinear non-Gaussian SSM, Briers et al. (2009) provided a discussion of the different smoothing approaches. This provides an idea about the structure of the smoothing distribution of the collection of states (Godsill et al., 2004). Filtering, on the other hand, aims to estimate the posterior expectation of the concentration value C_{t_i} , given the data up to t_i , i.e., $\{y(t_j) : j = 1, 2, \dots, i\}$. We have implemented both smoothing and filtering for all the physical models considered above.

To compare between models, we adopt a posterior predictive loss approach (see, e.g., Gelfand and Ghosh (1998)). We generate the posterior predictive distributions for each data point, $y_{rep,i}$ for $i = 1, 2, \dots, n$ by sampling from $p(y_{rep} | y) = \int p(y_{rep} | \theta, \{C_t\})p(\theta, \{C_t\} | y)d\theta$, where θ denotes the full collection of unknown parameters and $\{C_t\}$ is the collection of latent concentrations over the entire time frame. We will compute the posterior predictive mean, $\mu_{rep,i} = E[y_{rep,i} | y]$, and dispersion, $\Sigma_{rep,i} = \text{var}[y_{rep,i} | y]$, for each $y_{rep,i}$; these are easily calculated from the posterior samples for each $y_{rep,i}$. We will prefer models that will perform well under a decision-theoretic *balanced loss function* that penalizes departure of

replicated means from the corresponding observed values (lack of fit), as well as the uncertainty in the replicated data. Using a squared error loss function, the measures for these two criteria are evaluated as $G = \sum_{i=1}^n \|y_i - \mu_{rep,i}\|^2$, where $\|\cdot\|$ denotes the Euclidean norm, and $P = \sum_{i=1}^n \text{Tr}(\Sigma_{rep,i})$, where $\text{Tr}(A)$ denotes the trace of the matrix A . We will use the score $D = G + P$ as a model selection criteria, with lower values of D indicating better models.

4 Data Analysis

In this section we evaluate the performance of the models discussed in Section 3, for the three physical exposure models illustrated in Section 2, using computer-simulated datasets as well as experimental lab-generated data. In particular, we consider two models: a Gaussian linear model and a non-Gaussian nonlinear model, and they will be referred to as Gaussian SSM and non-Gaussian SSM respectively. The prior settings are based on physical knowledge and experience, and discussed in the following section.

The computer-simulated data was generated using R computing environment. The lab-generated data experiments were conducted in test chambers. Arnold et al. (2017) examined parts of this data using the deterministic one-zone and two-zone models and showed that performance is highly reliable on the model assumptions and knowing the generation (G) and ventilation (Q) rates. Shao et al. (2017) studied the eddy diffusion data using a deterministic model and concluded that it is suitable for indoor spaces with persistent directional flow toward a wall boundary, as well as in rooms where the airflow is solely driven by mechanical ventilation (no natural ventilation involved). These results imply the need for a more flexible model that accounts for uncertainty and also be used for parameter inference.

4.1 Prior settings

In Bayesian exposure models, reasonable informative priors are usually used, based on expert knowledge and physical considerations (Monteiro et al., 2014). We assigned informative priors on the generation rate G , ventilation rate Q , loss rate K_L , airflow rate β and

diffusion coefficient D_T using uniform distributions for the plausible values of the parameters. For the simulation data, uniform priors were assigned within at least 20% of the true values following the prior settings in Monteiro et al. (2011). The model parameters used to generate the one-zone model data were taken from physical considerations as illustrated by Zhang et al. (2009) at values, $Q = 13.8 \text{ m}^3/\text{min}$, $G = 351.5 \text{ mg}/\text{min}$, $V = 3.8 \text{ m}^3$, $K_L = 0.1 \text{ mg}/\text{min}$ and $\sigma = 0.1$. In the two-zone model, following Zhang et al. (2009), the generation and ventilation rates were fixed at the same values as in the one-zone model. In addition, β was fixed at $5 \text{ m}^3/\text{min}$, $V_N = \pi \times 10^{-3} \text{ m}^3$, $V_F = 3.8 \text{ m}^3$, and $\Sigma_\nu = \begin{bmatrix} 0.1 & 0 \\ 0 & 0.1 \end{bmatrix}$. For the eddy diffusion data, we fixed $G = 351.5 \text{ mg}/\text{min}$, $D_t = 1 \text{ m}^2/\text{min}$, $\sigma_\eta^2 = 0.1$ and used a geostatistical exponential covariance with $\sigma = \phi = 1$.

In the one-zone and two-zone models, we assume that $G \sim Unif(281, 482)$, $Q \sim Unif(11, 17)$, $K_L \sim Unif(0, 1)$, and $\beta \sim Unif(0, 10)$ in the two-zone model and $D_T \sim Unif(0, 3)$ in the eddy diffusion model. For the exponential covariance function, the spatial range is given by approximately $3/\phi$ which is the distance where the correlation drops below 0.05. The prior on $\phi \sim Uni(0.5, 3)$ implies that the effective spatial range, i.e., the distance beyond which spatial correlation is negligible, is between 1 and 6 units.

Wider ranges were considered in the lab-generated data analysis because the exact true values for some of the parameters were unknown but rather a range. The ranges of the true values in the well mixed compartment and two-zone models for G , Q , K_L and β are $(40 - 120)(\text{mg}/\text{min})$, $(0.04 - 0.77)(\text{m}^3/\text{min})$, < 0.01 and $(0.24 - 1.24)(\text{m}^3/\text{min})$ respectively. We assume that $G \sim Unif(30, 150)$, $Q \sim Unif(0, 1)$, $K_L \sim Unif(0, 1)$ in the one-zone and two-zone models and $\beta \sim Unif(0, 5)$ in the two-zone model. For the eddy diffusion model, the true value for G is 1318 (mg/sec) and from literature (Shao et al., 2017) the range for D_T is $(0.001-0.2) \text{ m}^2/\text{sec}$, hence we assigned priors of $G \sim Unif(1104, 1650)$ and $D_t \sim Unif(0, 1)$. Non informative priors were assigned to the variance covariance matrices using $IW(3, I)$ (Gelman et al., 2013).

4.2 Simulation results

Monte Carlo filtering methods were used to estimate the latent processes and the model parameters. The effectiveness of the model is assessed through checking whether the 95% C.I.s of the parameters include the true values, MSE and posterior predictive loss (D=G+P), in addition to graphical assessment.

4.2.1 One-zone model

We simulated 100 exposure concentrations at equally spaced time points using the exact solution to the ODE in equation (2). The initial concentration $C(0)$ was assigned a value of 1 mg/m³. Theoretically, the steady state concentration is $G/Q \approx 25$ mg/m³. The models applied to the synthetic data and compared are: Gaussian SSM and non-Gaussian SSM. The Gaussian SSM in (8) assumes linearity and Gaussian errors, where the Kalman filter equations are used, where

$$A_t(\theta_c) = \left(1 - \delta_t \frac{Q + K_L V}{V}\right) \quad \text{and} \quad g = \delta_t \frac{G}{V}.$$

Table 1 shows the medians and 95% credible intervals of the MCMC posterior samples of the model parameters, MSE and D=G+P for the two aforementioned models. Figure 4 shows the simulated concentrations, measurements and the mean of the posterior samples of the latent states conditional on the measurements, in addition to smoothed estimates obtained from the Non-Gaussian SSM filtered states. Details of the performances are as follows:

- Non-Gaussian SSM: The 95% C.I.s include the true values for all the parameters except K_L . The latent state estimates are very close to the true simulated values as shown in Figure 4.
- Gaussian SSM: The 95% C.I.s for the generation rate G and the ventilation rate Q include the true values. The interval for the loss rate K_L does not cover the true parameter value. The model estimates for the latent states are closer to the observed values than the true values.

The $D=G+P$ scores and MSE results suggest that the nonlinear non-Gaussian model outperforms the linear Gaussian one, which is also confirmed in Figure 4.

Table 1: Posterior predictive loss ($D=G+P$), MSE, medians and 95% C.I. of the posterior samples of the one-zone model parameters for the simulated data

Parameter	Non-Gaussian SSM	Gaussian SSM
$G(351.5)$	326.8 (283.3, 351.7)	363.5(314.2,413.8)
$Q(13.8)$	12.9(11.1, 14.8)	12.8(11.4, 14.3)
$K_L(0.1)$	0.34(0.19,0.78)	0.30(0.28, 0.41)
$D=G+P$	312.2=5.9+306.3	435.8=232.8+203.0
MSE	0.07	2.3

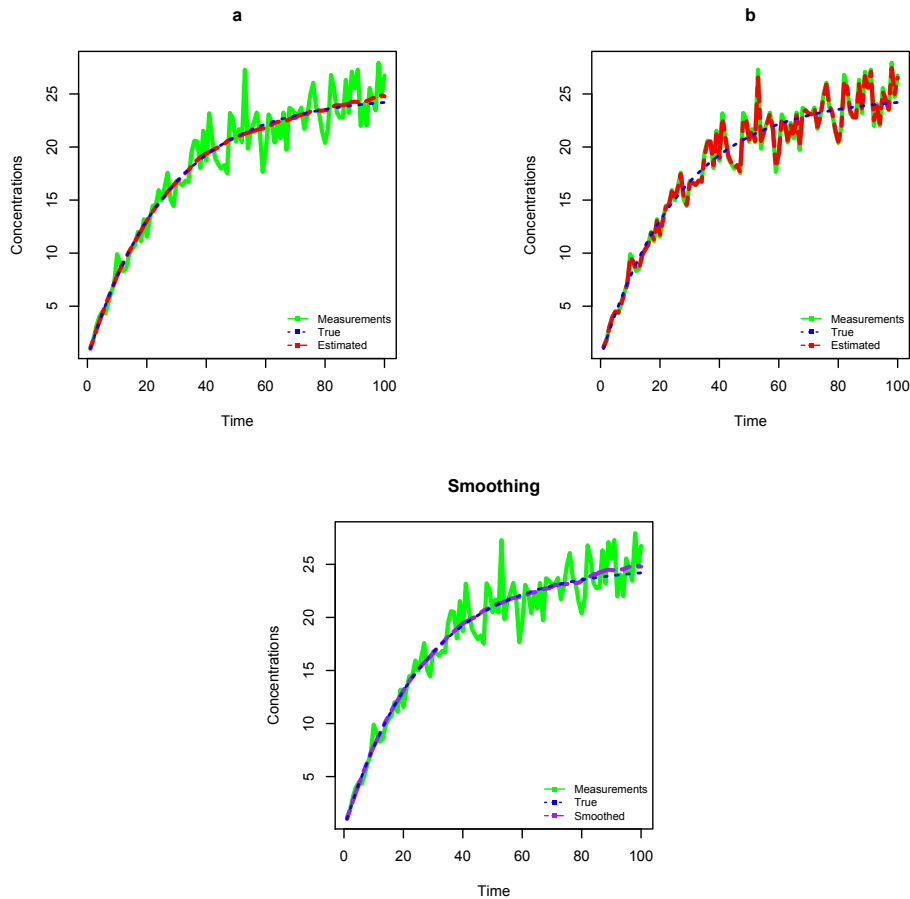


Figure 4: Plot of the simulated concentrations, measurements and the mean of the posterior samples of the latent states conditional on the measurements for:
a: Non-Gaussian SSM and b: Gaussian SSM

4.2.2 Two-zone model

We simulated 100 exposure concentrations at the near and far fields at equally spaced time points using the exact solution (5). The initial concentrations $C_N(0)$ and $C_F(0)$ were assigned values 0 and 0.5 mg/m³ respectively. Theoretically, the steady state concentration at the near field is $G/Q + G/\beta \approx 95$ mg/m³, and $G/Q \approx 25$ mg/m³ at the far field. The Gaussian SSM in (8) assumes linearity and Gaussian errors, such that

$$A_t(\theta_c) = \delta_t A + I \quad \text{and} \quad g = \delta_t g.$$

Table 2 shows the medians and 95% C.I.s of the MCMC posterior samples of the model parameters, MSE and D=G+P scores. Figure 5 shows the simulated concentrations, measurements and the mean of the posterior samples of the latent states conditional on the measurements at the near and the far fields in addition to smoothed estimates obtained from the non-Gaussian SSM filtered states. Moreover, we compared the performance of the two SSMs to the simple Bayesian nonlinear regression model (BNLR) proposed by Zhang et al. (2009). Details of the performances of the three models are as follows:

- Non-Gaussian SSM: The 95% C.I.s include the true values for all the parameters. The estimates of the latent states are close to the true values at both the near field and the far field as shown in Figure 5.
- Gaussian SSM: The 95% C.I.s for all the parameters except the ventilation rate Q do not include the true values. The model estimates of the latent states are closer to the true values at the near field than the far field.
- BNLR: The 95% C.I.s include the true values for all the parameters.

The D=G+P scores indicate that the non-Gaussian model provides better fit than the BNLR and the Gaussian models. MSE and Figure 5 confirm these results.

4.2.3 Turbulent eddy diffusion model

We simulated a total of 500 exposure concentrations at 5 different locations over equally spaced 100 time points using the exact equation (6). Table 3 shows the medians and 95%

Table 2: Posterior predictive loss (D=G+P), MSE, medians and 95% C.I. of the posterior samples of the two-zone model parameters for the simulated data

Parameter	Non-Gaussian SSM	Gaussian SSM	BNLR
$G(351.5)$	347.3(315.6,379.3)	450.5(395.2, 480.2)	335.1(302.5,382.6)
$Q(13.8)$	14.7(12.1,16.8)	13.5(11.1, 16.7)	14.4(11.2, 15.8)
$K_L(0.1)$	0.38(0.02,0.78)	0.22(0.16,0.35)	-
$\beta(5)$	5.0(4.3,5.8)	0.40(0.23,1.2)	5.1(4.0, 6.8)
D=G+P	1049840=	1118550=	2504429=
	1010905+38934.0	1033428+85121.7	1359016+ 1145413
MSE	15.3	116.1	54.9

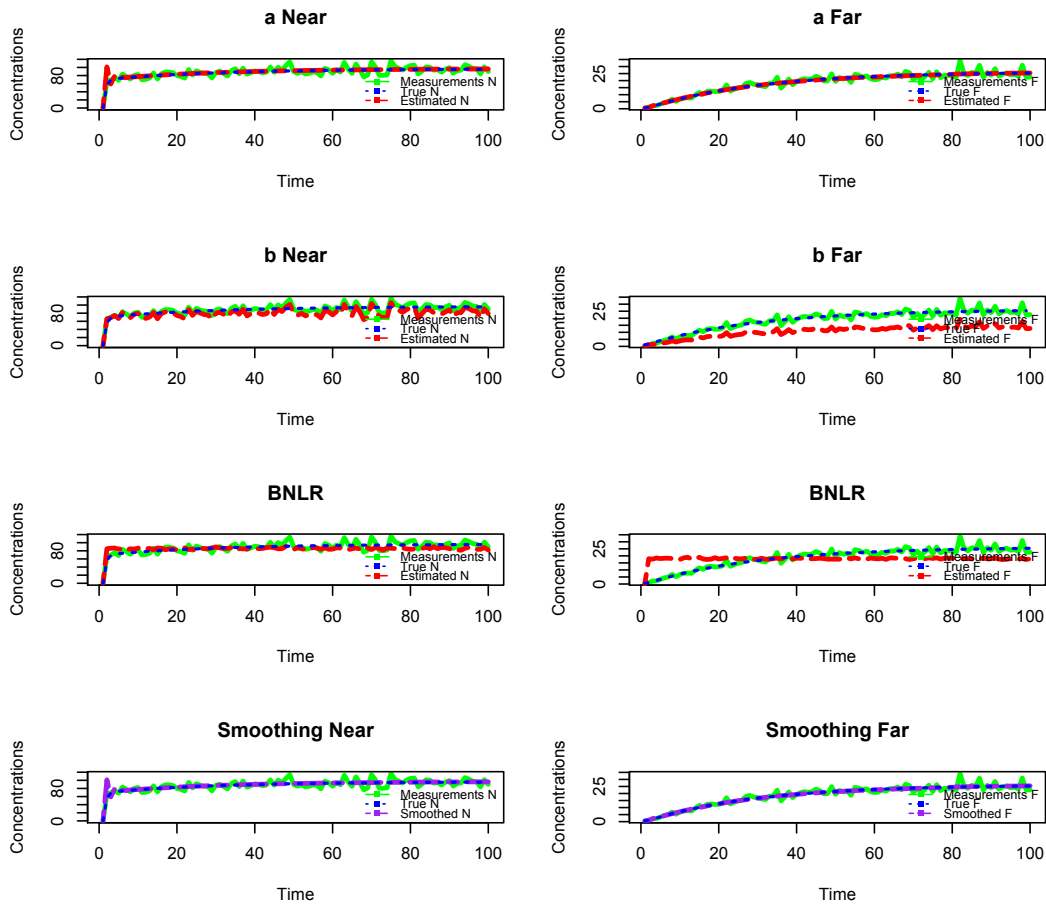


Figure 5: Plot of the simulated near and far fields concentrations, measurements and the mean of the posterior samples of the latent states conditional on the measurements for: a: Non-Gaussian SSM, b: Gaussian SSM and BNLR

C.I.s of the MCMC posterior samples of the model parameters, MSE and D=G+P. Figure 6 shows the simulated concentrations, measurements and the mean of the posterior samples of the latent states conditional on the measurements at three locations and the smoothed estimates obtained from the non-Gaussian SSM filtered states. Figure 7 shows image plot of the posterior mean surface of the latent spatial process $\nu_t(s)$. The plot indicates higher concentration values near the source of emission at the bottom-left corner and lower values away from the source. Details of the performance of the two models are as follows:

- Non-Gaussian SSM: The 95% C.I.s include the true values for all the parameters. The estimates of the latent states are close to the true values at the five locations.
- Gaussian SSM: The 95% C.I.s include the true value for the generation rate G but not for the eddy diffusion coefficient D_T . The model estimates for the latent states are closer to the observed values than the true values.

MSE and D=G+P for the Non-Gaussian SSM indicate a better fit.

Table 3: Posterior predictive loss (D=G+P), MSE, medians and 95% C.I of the posterior samples of the turbulent eddy diffusion model parameters for the simulated data

Parameter	Non-Gaussian SSM	Gaussian SSM
$G(351.5)$	355.9(284.0,477.5)	449.6(301.0,480.5)
$D_T(1)$	1.2(0.9,1.5)	1.4(1.3,1.6)
D=G+P	7062.4=1564.5+5497.9	22025.7=1112.5+20913.1
MSE	3.11	5.55

4.3 Experimental Chamber Data Results

In this section we study the performance of the non-Gaussian and Gaussian SSMs on controlled lab-generated data in which solvent concentrations have been measured under different scenarios. We are interested in the inference through the posterior distributions of the parameters Q and G in the one-zone model, in addition to β in the two-zone model, and Q and D_T in the eddy diffusion model.

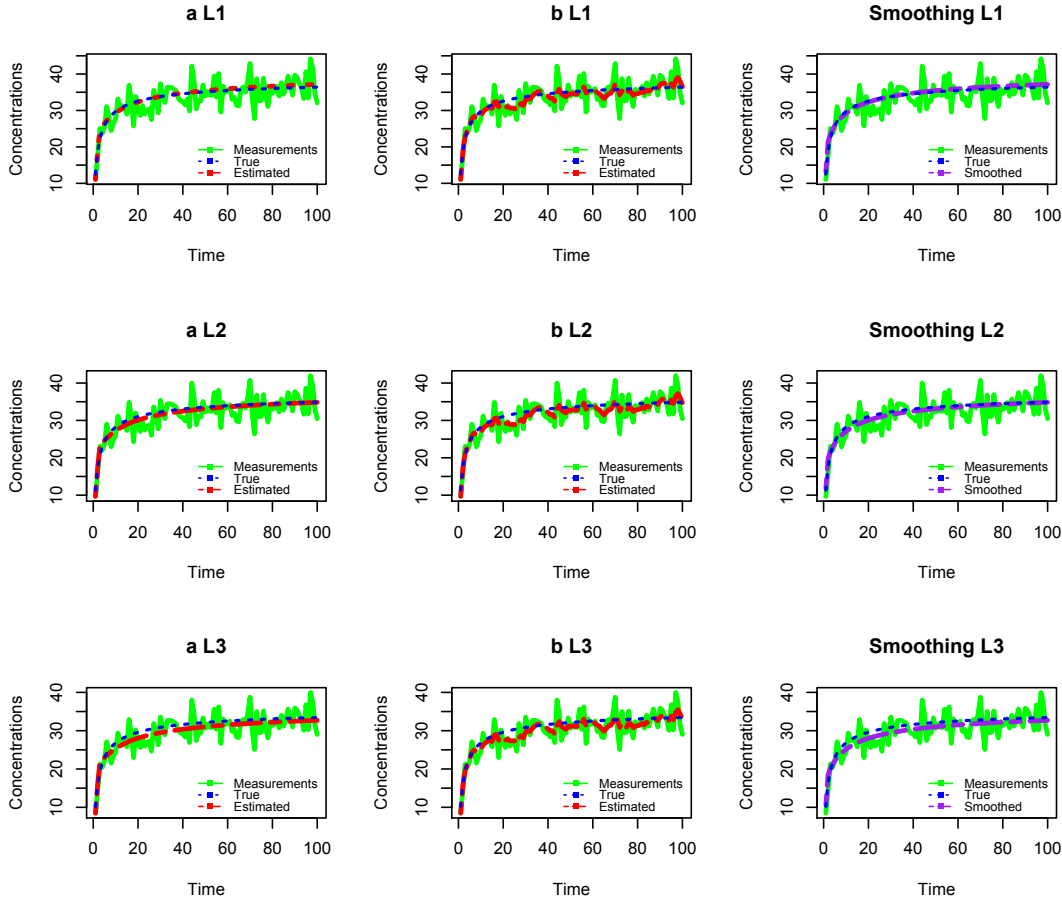


Figure 6: Plot of the simulated concentrations, measurements and the mean of the posterior samples of the latent states conditional on the measurements at three locations for:
a: Non-Gaussian SSM and b: Gaussian SSM

4.3.1 One-zone model

A series of studies were conducted in an exposure chamber under different controlled conditions. Arnold et al. (2017) constructed a chamber of size $(2.0\text{m} \times 2.8\text{m} \times 2.1\text{m} = 11.8\text{m}^3)$, where two industrial solvents (acetone and toluene) were released using different generation $G(\text{mg}/\text{min})$ and ventilation $Q(\text{m}^3/\text{min})$ rates. In particular, three levels of ventilation rates corresponding to ranges of $0.04\text{-}0.07 \text{ m}^3/\text{min}$, $0.23\text{-}0.27 \text{ m}^3/\text{min}$ and $0.47\text{-}0.77 \text{ m}^3/\text{min}$ were used. The loss rate K_L was determined from empirical studies to be < 0.01 . Solvent concentrations were measured every 1.5 minutes. Details of the experiments can be found in (Arnold et al., 2017).

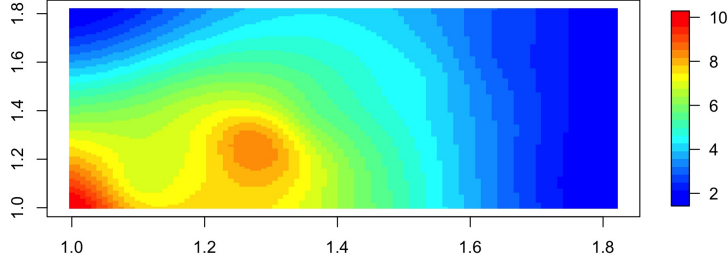


Figure 7: Interpolated surface of the mean of the random spatial effects posterior distribution

Table 4 shows the medians and 95% C.I.s of the MCMC posterior samples in addition to MSE and $D=G+P$. The non-Gaussian SSM 95% C.I.s cover the true values for both G and Q , while Gaussian SSM 95% C.I.s include the true values for G at low and high ventilation levels. Figure 8 shows that the estimated latent concentrations are close to the measurements. Posterior predictive loss ($D=G+P$) indicates better fit of the non-Gaussian SSM model.

Table 4: Posterior predictive loss ($D=G+P$), MSE, medians and 95% C.I. of the posterior samples of the one-zone model parameters using toluene and acetone solvents

Parameter	Ventilation level	True value	Non-Gaussian SSM	Gaussian SSM
G	low	43.2	38.1(30.2,62.9)	35.3(30.2, 46.7)
	medium	43.2	45.06(30.5,101.9)	72.9(45.6,94.9)
	high	39.55	81.7(32.9,142.4)	38.1(30.5,51.4)
Q	low	0.04-0.07	0.27(0.02, 0.41)	0.20(0.15,0.27)
	medium	0.23-0.27	0.50(0.02,0.97)	0.15(0.10,0.21)
	high	0.47-0.77	0.59(0.03,0.98)	0.30(0.23,0.45)
$D=G+P$	low		129.4=88.8+40.6	208.0=4.3+203.7
	medium		9.8=0.52+9.2	77.7=0.20+77.1
	high		7.5=1.0+6.5	38.2=0.1+38.1
MSE	low		0.01	0.02
	medium		0.02	0.02
	high		0.03	0.02

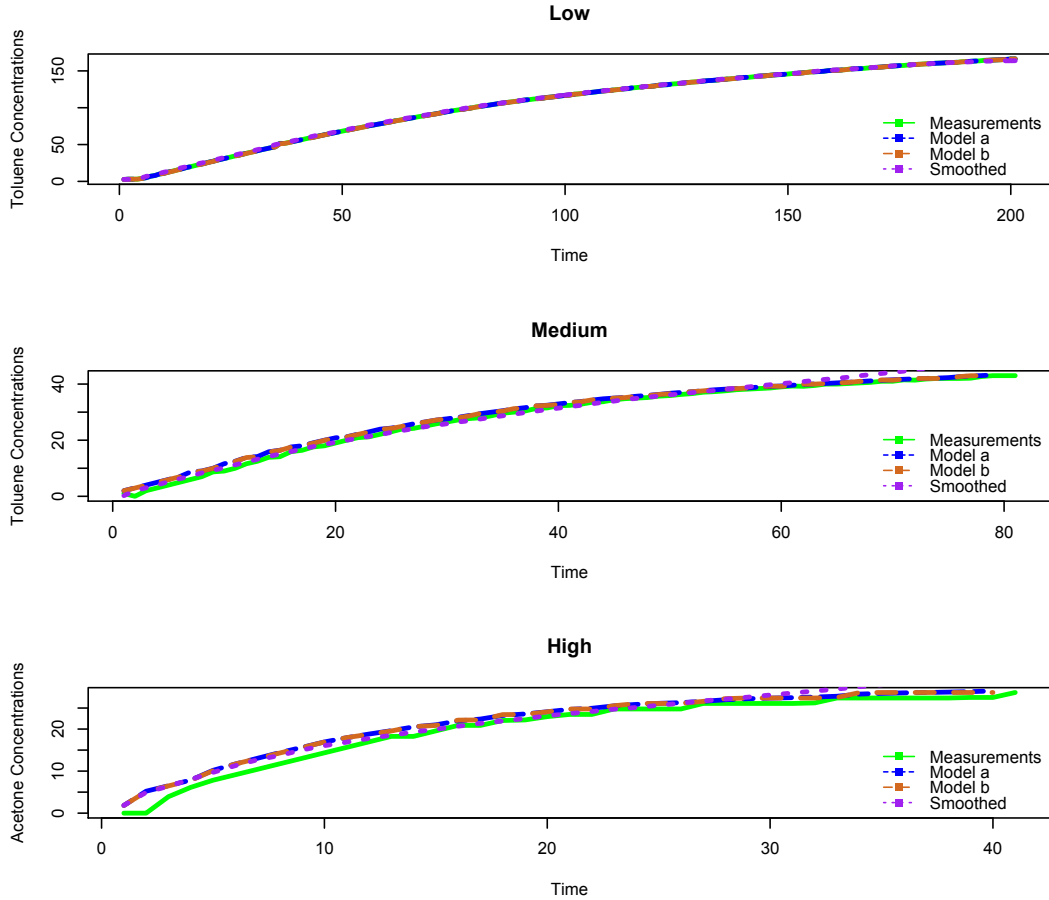


Figure 8: Plot of the measured concentrations and the mean of the posterior samples of the latent states conditional on the measurements for:
a: Non-Gaussian SSM and b: Gaussian SSM

4.3.2 Two-zone model

The near field box of size $(0.51\text{m} \times 0.51\text{m} \times 0.41\text{m} = 0.105\text{m}^3)$ was constructed within the far field box (Arnold et al., 2017). The volume of the far field is 11.79 m^3 , which is the chamber volume minus the near field volume. The airflow parameter β cannot be directly measured, but it was estimated from the local air speed to range from 0.24 to 1.24 m^3/min . Similar to the one-zone model, three different experimental data sets at three different ventilation levels were used. Table 5 shows the medians and 95% C.I.s of the MCMC posterior samples, MSE and $D=G+P$. At all ventilation rates, non-Gaussian SSM 95% C.I.s include the true values of Q but only at a medium ventilation rate, it includes the true value for G . The Gaussian SSM 95% C.I.s cover the true value of Q at medium

ventilation level but none of the generation rates G . The BNLR 95% C.I.s only cover the true value of Q at a high ventilation level. The true value for β was not directly measured and hence is unknown, however, it was estimated to be between 0.24 and 1.24. In general, non-Gaussian SSM 95% C.I.s for β are closer to those values.

MSE and D=G+P scores clearly indicate that non-Gaussian SSM produced better fit than the BNLR and the Gaussian SSM which is also confirmed in Figure 9.

Table 5: Posterior predictive loss (D=G+P), MSE, medians and 95% C.I. of the posterior samples of the two-zone model parameters using toluene and acetone solvents

Parameter	Ventilation level	True value	Non-Gaussian SSM	Gaussian SSM	BNLR
G	low	43.2	30.4(30.0, 32.2)	115.8(88.9, 143.9)	28.1(28.0,28.4)
	med	86.4	73.7(60.2,90.5)	141.6(130.6,149.7)	28.5(28.0,30.8)
	high	120.7	49.8(33.9,68.3)	132.9(121.6,148.0)	43.7(37.8,50.3)
Q	low	0.04-0.07	0.68(0.09, 0.98)	0.28(0.23,0.36)	0.62(0.60,0.65)
	med	0.23-0.27	0.38(0.11,0.50)	0.25(0.20,0.31)	0.38(0.29,0.50)
	high	0.47-0.77	0.46(0.45,0.98)	0.14(0.11,0.16)	0.5(0.30,0.64)
β	low	0.24-1.24	3.0(2.3,3.7)	5.1(4.1,6.0)	4.9(4.7,5.0)
	med	0.24-1.24	2.9(2.5, 3.4)	2.3(2.0,2.8)	4.5(3.4,5.0)
	high	0.24-1.24	2.2(1.5, 2.8)	2.5(2.0,3.0)	4.1(2.7,4.9)
D=G+P	low		5653=	554650=	248358=
	medium		189+5464	554234+416	73006+ 175352
			22262=	850014=	93267=
	high		10596+11666	424452+425562	16824+76443
		20941=	479098=	119212=	
		4345+16596	240278+238820	64968+54244	
MSE	low		0.62	1835.2	129.2
	medium		13.0	2952.4	96.5
	high		52.9	2930.2	632.3

4.3.3 Turbulent eddy diffusion model

Shao et al. (2017) constructed a chamber of size ($2.8\text{m} \times 2.15\text{m} \times 2.0\text{m} = 11.9\text{m}^3$), where toluene was released. Measurements were taken at two locations at distances 0.41 m and 1.07 m away from the source every two minutes. Due to the limited spatial information from the two locations, an unstructured covariance for $\nu_t(s)$ was used instead of the geostatistical exponential covariance that was considered in the simulation analysis. Non informative

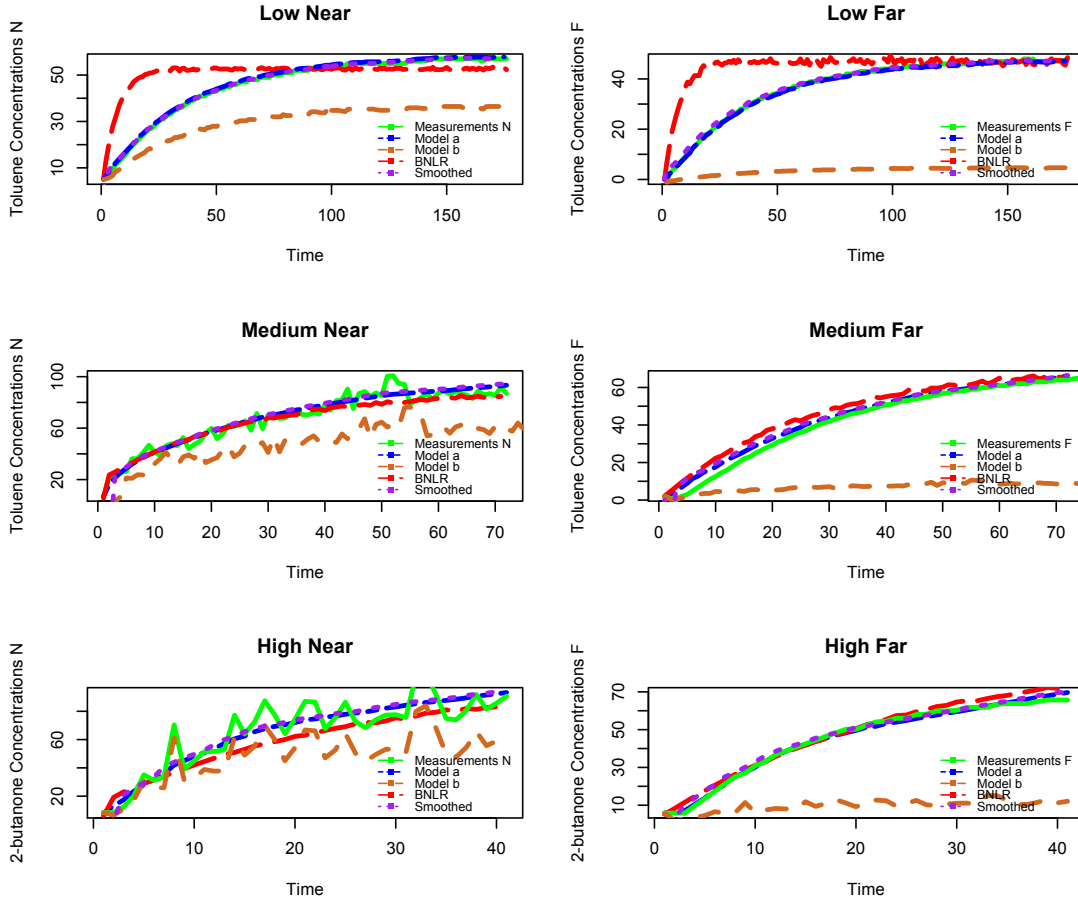


Figure 9: Plot of the measured concentrations and the mean of the posterior samples of the latent states conditional on the measurements in the near field and far field for:
a: Non-Gaussian SSM, b: Gaussian SSM and BNLR

prior was assigned to the covariance matrix using $IW(3, I)$ (Gelman et al., 2013).

Table 6 shows the medians and 95% C.I.s of the MCMC posterior samples, MSE and the $D=G+P$. The value of D_T is difficult to measure; hence, the true value is unknown. However, Shao et al. (2017) demonstrated that most of the reported values of D_T in literature range from 0.001 to 0.01 m^2/sec . The 95% C.I.s for D_T in non-Gaussian SSM lie within that range. In addition, the 95% C.I.s of G include the true value. The 95% C.I.s of the Gaussian SSM do not include any of the true parameter values. Figure 9 shows that the latent state estimates for both models are closer to the measurements in the first location than in the second location. MSE and $D=G+P$ scores show that non-Gaussian SSM provides a better fit.

Table 6: Posterior predictive loss ($D=G+P$), MSE, medians and 95% C.I. of the posterior samples of the turbulent eddy diffusion model parameters using toluene solvent

Parameter	True value	Non-Gaussian SSM	Gaussian SSM
G	1318.33	1207.3(1107.2,1371.7)	1118.7(1104.5,1294.3)
D_T	0.001-0.01	0.007(0.006,0.008)	0.67(0.64,0.78)
$D=G+P$		100877.8=59369.9+41507.9	32383410=258952.4+32124457
MSE		337.3	1454.8

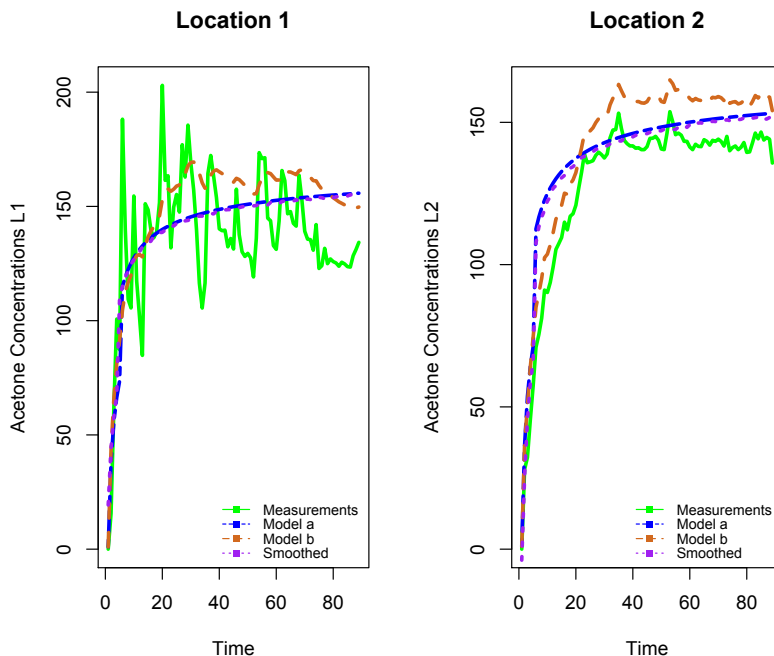


Figure 10: Plot of the measured concentrations and the mean of the posterior samples of the latent states conditional on the measurements at the two locations for:
a: Non-Gaussian SSM and b: Gaussian SSM

5 Discussion

We have proposed a framework of Bayesian SSMs for analyzing experimental exposure data specific to industrial hygiene. This approach combines information from physical models of industrial hygiene, observed data and prior information. We derive a likelihood by discretizing the physical models. It also expands upon the Gaussian noise assumptions, hence industrial hygienists will not be restricted to Gaussian SSMs.

In practical industrial hygiene settings, Gaussian SSMs are still often used as approximations to analyze possibly non-Gaussian data. To do so, some possibly inappropriate accommodations may need to be made. For example, Hoi et al. (2008) allowed negative values in estimating PM₁₀ concentrations, while Leleux et al. (2002) used Kalman filters to predict gas concentrations by using a tuning parameter to fix σ_ω^2 and σ_ν^2 in a one dimensional autoregressive exposure model, rather than pursuing full statistical inference. Our simulation experiments and results demonstrate that Gaussian SSM’s may yield extremely poor fits when data are non-Gaussian. This was especially evident for the two-zone analysis. Our results will, we hope, inform the industrial hygiene community about some of the pitfalls of Gaussian SSMs.

Non-Gaussian SSM’s tended to perform better than linear Gaussian SSM’s, a result that appeared to be consistent across different exposure models and different experimental conditions. Moreover, our analysis of the two-zone data revealed that the discretized models outperform the BNLR method proposed by Zhang et al. (2009) for two zone data. This is unsurprising given that our approach is richer by accommodating stochastic distributions at two levels—one each for the measurement and transition equations—whereas BNLR accommodates only an error distribution from a nonlinear regression. Finally, our proposed approach also enjoys better interpretation than the hierarchical Gaussian process models of Monteiro et al. (2014) as they provide greater precisions in estimates because the random effects in the hierarchical models of Monteiro et al. (2014) tend to inflate variances.

The eddy diffusion data has some limitations related to the small size of the chamber, which rendered a small difference between the concentrations in the two locations which also makes it hard to measure the spatial variation for Model (7) implementation. Despite that, in most cases, a nonlinear non-Gaussian Bayesian SSM was able to characterize the data well and the model seems robust to most of the experimental scenarios.

We conclude with some indicators for future research. First, as alluded to earlier, we will need to do a much more comprehensive spatiotemporal analysis for eddy diffusion experiments. While our simulation experiments showed the promise of spatiotemporal SSM’s in analyzing eddy diffusion experiments, our chamber data analysis had limited scope because of the very small number of spatial measurements. Another important

consideration is misaligned data, such as was considered in Monteiro et al. (2014) for two zone experiments where not all measurements for the near and far fields came from the same set of timepoints. An advantage of the Bayesian paradigm is that we can handle missing data, hence misaligned data, very easily and indeed our Bayesian SSMs should be able to handle them as easily as the models in Monteiro et al. (2014). Future work will include such analysis and also extensions to spatiotemporal misalignment for eddy-diffusion experiments, where not all timepoints generated measurements for the same set of spatial locations.

SUPPLEMENTARY MATERIAL

R-code for Bayesian SSMs used: R- code to perform the filtering, smoothing and parameters estimation and model assessment methods described in the article. (BSTSP Rmd file)

Discretization of the differential equations: We approximate the deterministic physical model through discretization. The Taylor expansion of $C(t)$ at $t = t^*$ is $C(t) = \sum_{n=0}^{\infty} \frac{C^{(n)}(t^*)}{n!} (t - t^*)^n$, where $C^{(n)}(t^*) = \left. \frac{d^n}{dt^n} C(t) \right|_{t=t^*}$. Let $t = t^* + \delta_t$ hence

$$C(t^* + \delta_t) = \sum_{n=0}^{\infty} \frac{C^{(n)}(t^*)}{n!} (\delta_t)^n = C(t^*) + \frac{C'(t^*)}{1!} \delta_t + o(\delta_t), \quad (9)$$

for small δ_t . From the above equation we can express $C'(t^*)$ as

$$C'(t^*) = \frac{C(t^* + \delta_t) - C(t^*)}{\delta_t} + o(\delta_t). \quad (10)$$

In the applications to the three physical models we replace the first order derivative $\frac{d}{dt}C(t)$ at $t = t^*$ with equation (10) using the appropriate value of δ_t . In the one zone and two-zone models a value $\delta_t = 0.01$ was found to provide an accurate approximation, while for the eddy diffusion model $\delta_t = 1$ was used.

Steady states derivations: The steady state is achieved as $t \rightarrow \infty$ in the exact solution of the ODE.

$$\lim_{t \rightarrow \infty} \exp\{tF_t\} C(t_0) + F_t^{-1} [\exp\{tF_t\} - I] g. \quad (11)$$

For the one zone model $F_t = -(Q + K_L V)/V$ and $g = G/V$ so $11 = F_t^{-1} [-I] g = G/(Q + K_L V)$. Since K_L is usually small, it can be approximated by G/Q . Hence as $t \rightarrow \infty$ $C(t) \approx G/Q$.

For the two zone model, $F_t = A = \begin{bmatrix} -\beta/V_N & \beta/V_N \\ \beta/V_F & -(\beta + Q)/V_F + K_L \end{bmatrix}$ and $g =$

$\begin{bmatrix} G/V_N \\ 0 \end{bmatrix}$. Since K_L is usually small it can be ignored for simplicity. The term $\exp(tF_t)$, where $\exp()$ is the matrix exponential, can be written as $\exp(tL\Lambda L^{-1}) = \sum e^{t\lambda} G_i$ where $G_i = u_i v_i^T$, u_i is the i -th column of L and v_i^T is the i -th row of L^{-1} . It easily follows that $e^{tFt} = \sum_{i=1}^m e^{t\lambda_i} G_i$. The eigenvalues are available in closed form Zhang et al. (2009) as

$$\begin{aligned}
\lambda_1 &= \frac{1}{2} \left[- \left(\frac{\beta V_F + (\beta + Q) V_N}{V_N V_F} \right) + \sqrt{\left(\frac{\beta V_F + (\beta + Q) V_N}{V_N V_F} \right)^2 - 4 \left(\frac{\beta Q}{V_N V_F} \right)} \right], \\
\lambda_2 &= \frac{1}{2} \left[- \left(\frac{\beta V_F + (\beta + Q) V_N}{V_N V_F} \right) - \sqrt{\left(\frac{\beta V_F + (\beta + Q) V_N}{V_N V_F} \right)^2 - 4 \left(\frac{\beta Q}{V_N V_F} \right)} \right].
\end{aligned} \tag{12}$$

As long as β and Q are positive, the sum of the two eigenvalues are negative. Hence $e^{tFt} = \sum_{i=1}^m e^{t\lambda_i} G_i \rightarrow 0$ as $t \rightarrow \infty$ and the first term becomes 0 and the second term becomes $A^{-1}[-I]g$. The determinant of A is $\det(A) = Q\beta/V_N V_F$, and $A^{-1} = \begin{bmatrix} -((\beta + Q)/V_F)(V_N V_F/\beta Q) & -(\beta/V_N)(V_N V_F/\beta Q) \\ -(\beta/V_F)(V_N V_F/\beta Q) & -((\beta)/V_N)(V_N V_F/\beta Q) \end{bmatrix}$. So the steady state is a 2×1 vector equal to $A^{-1}[-I]g = \begin{bmatrix} \frac{G}{Q} + \frac{G}{\beta} \\ \frac{G}{Q} \end{bmatrix}$. So as $t \rightarrow \infty$ $C_N(t) \approx \frac{G}{Q} + \frac{G}{\beta}$ and $C_F(t) \approx \frac{G}{Q}$.

The steady state for the eddy diffusion model is theoretically the value of $C(s, t)$ in equation (6) when $t \rightarrow \infty$. Clearly $\lim_{t \rightarrow \infty} \frac{G}{2\pi D_T(\|s\|)} \left(1 - \operatorname{erf} \frac{\|s\|}{\sqrt{4D_T t}} \right) = \frac{G}{2\pi D_T(\|s\|)}$.

References

- Arnold, S., Shao, Y., and Ramachandran, G. (2017). Evaluating well-mixed room and near-field-far-field model performance under highly controlled conditions. *Journal of Occupational and Environmental Hygiene* **14**, 427–437.
- Banerjee, S., Carlin, B. P., and Gelfand, A. E. (2014). *Hierarchical Modeling and Analysis for Spatial Data*. Chapman and Hall/CRC.
- Banerjee, S., Ramachandran, G., Vadali, M., and Sahmel, J. (2014). Bayesian hierarchical framework for occupational hygiene decision making. *The Annals of Occupational Hygiene* **58**, 1079–1093.
- Banerjee, S. and Roy, A. (2014). *Linear Algebra and Matrix Analysis for Statistics*. Chapman and Hall/CRC.
- Briers, M., Doucet, A., and Maskell, S. (2009). Smoothing algorithms for state-space models. *Annals of the Institute of Statistical Mathematics* **62**, 61–89.
- Eubank, R. L. (2005). *A Kalman Filter Primer*. Chapman and Hall/CRC.
- Fearnhead, P. (2011). *MCMC for state-space models*, pages 513–529. Chapman and Hall.
- Gelfand, A. E., Banerjee, S., and Gamerman, D. (2005). Spatial process modelling for univariate and multivariate dynamic spatial data. *Environmetrics* **16**, 465–479.
- Gelfand, A. E. and Ghosh, S. K. (1998). Model choice: A minimum posterior predictive loss approach. *Biometrika* **85**, 1–11.
- Gelman, A., Carlin, J. B., Stern, H. S., Dunson, D. B., Vehtari, A., and Rubin, D. B. (2013). *Bayesian Data Analysis*. Chapman and Hall/CRC.
- Godsill, S. J., Doucet, A., and West, M. (2004). Monte carlo smoothing for nonlinear time series. *Journal of the American Statistical Association* **99**, 156–168.
- Hoi, K., Yuen, K., and Mok, K. (2008). Kalman filter based prediction system for winter-time pm10 concentrations in macau. *Global NEST Journal* **10**, 140–150.

- Katfuss, M., Stroud, J. R., and Wikle, C. K. (2016). Understanding the ensemble kalman filter. *The American Statistician* **70**, 350–357.
- Keil, C. B., Berge, W. F. T., and AIHA (2009). *Mathematical models for estimating occupational exposure to chemicals*. AIHA Press.
- Leleux, D., Claps, R., Chen, W., F.K.Tittel, and Harman, T. (2002). Applications of kalman filtering to real-time trace gas concentration measurements. *Applied Physics B* **74**, 85–93.
- Monteiro, J. V. D., Banerjee, S., and Ramachandran, G. (2011). B2z: An r package for bayesian two-zone models. *Journal of Statistical Software* **43**,.
- Monteiro, J. V. D., Banerjee, S., and Ramachandran, G. (2014). Bayesian modeling for physical processes in industrial hygiene using misaligned workplace data. *Technometrics* **56**, 238–247.
- Nicas, M. and Jayjock, M. (2002). Uncertainty in exposure estimates made by modeling versus monitoring. *AIHA Journal* **63**, 275–283.
- Ramachandran, G. (2005). *Occupational Exposure Assessment for Air Contaminants*. CRC Press.
- Shao, Y., Ramachandran, S., Arnold, S., and Ramachandran, G. (2017). Turbulent eddy diffusion models in exposure assessment - determination of the eddy diffusion coefficient. *Journal of Occupational and Environmental Hygiene* **14**, 195–206.
- Wikle, C. K. and Cressie, N. (1999). A dimension-reduced approach to space-time kalman filtering. *Biometrika* **86**, 815–829.
- Zhang, Y., Banerjee, S., Lungu, C., and Ramachandran, G. (2009). Bayesian modeling of exposure and airflow using two-zone models. *Annals of Occupational Hygiene* **53**, 409–424.